Even within the assumptions made in searching for a partial-wave fit, the present results do not by any means represent a complete search for different minima in χ^2. A more elaborate analysis and, probably, more accurate data will be required to give a definitive result.

ACKNOWLEDGMENTS

We would like to thank the 30-in. bubble chamber group for their help with the exposure, and the Columbia group for their work with the beam. We are indebted to the analysis teams at Pisa and BNL for their work. The Pisa group would like to thank Centro Studi Calcolatrici Elettroniche and Centro Nazionale Universitario di Calcolo Elettronico. We thank Dr. Philip Connolly, Dr. David Stonehill, Dr. Bernard Thevenet, and Dr. Francesco Pagni for their assistance in earlier phases of this work. Dr. C. Alff-Steinberger designed the separated beam used.

PHYSICAL REVIEW VOLUME 177, NUMBER 5 25 JANUARY 1969

Study of Neutral Final States Produced in π^-p Collisions at Momenta of 1.71–2.46 GeV/c

A. S. CARROLL*
Rutherford High Energy Laboratory, Chilton, Berkshire, England

AND

I. F. CORBETT, C. J. S. DAMERELL,† N. MIDDLEMAS, D. NEWTON,‡
A. B. CLEGG,‡ AND W. S. C. WILLIAMS
Nuclear Physics Laboratory, Oxford, England

(Received 24 June 1968)

We have studied neutral final states produced in π^-p collisions at momenta of 1.71, 1.89, 2.07, 2.27, and 2.46 GeV/c, by observing the γ rays emitted. In particular, measurements are presented of (i) $\pi^-p \to \pi^0 n$, for which the Regge-pole fit at momenta ≥ 5.9 GeV/c also agrees rather well here; (ii) $\pi^-p \to \eta^0 n$, for which the Regge model which fits at higher energies does not agree here; (iii) $\pi^-p \to \pi^0\gamma n$, in which there is some evidence for a diffraction dissociation process as well as ω^0-meson production; (iv) $\pi^-p \to \pi^0\pi^0 n$, which is dominated by production of $N^{*0}(1236)\pi^0$ and by peripheral production of pion pairs. In (iv), the former process is found to fit with the same Reggeized ρ-meson exchange model as charge-exchange scattering, while the latter gives indication of the s-wave $\pi\pi$ interaction. An account is given of new techniques, particularly in the data analysis, which were developed in the course of this work.

1. INTRODUCTION

THE results of a spark-chamber experiment which studied the neutral final states produced in π^-p collisions are reported by us. When a counter system showed that an incident pion disappeared, with no outgoing charged particles produced, spark chambers urrounding the target were triggered to detect γ rays produced. The experiment was initially designed to study charge-exchange scattering,

$$\pi^- + p \to \pi^0 + n, \tag{1}$$

in the neighborhood of the $N^*(2190)$ which was reported as a peak in the π^-p total cross sections.[1] However, it proved necessary to design the experiment so that it could also study reactions in which more than two γ rays are produced, and other interesting results have been obtained from study of these channels.

Some of the results of this work have been published previously. In a letter[2] we presented graphs of the angular distributions for charge-exchange scattering, demonstrating that they were very close to the angular distributions deduced from a Regge model using the same parameters as were found to fit the angular distributions at higher momenta from 5.9 to 18.2 GeV/c. It is of course surprising that the Regge model should work at all well at the momenta of our experiment. We also showed[2] that the same Regge model fitted well the angular distribution found for the reaction

$$\pi^- + p \to \pi^0 + [N^{*0}(1238) \to n + \pi^0] \tag{2}$$

in our experiment. The fit to the charge-exchange angular distributions was not perfect, but the discrepancy was such as could be explained by interference

* Present address: Brookhaven National Laboratory, Upton, N. Y.
† Present address: Rutherford High Energy Laboratory, Chilton, Berkshire, England.
‡ Present address: University of Lancaster, Lancaster, England.
[1] A. N. Diddens, E. W. Jenkins, T. F. Kycia, and K. F. Riley, Phys. Rev. Letters **10**, 262 (1963).
[2] A. S. Carroll, I. F. Corbett, C. J. S. Damerell, N. Middlemas, D. Newton, A. B. Clegg, and W. S. C. Williams, Phys. Rev. Letters **16**, 288 (1966); **17**, 1274(E) (1966).

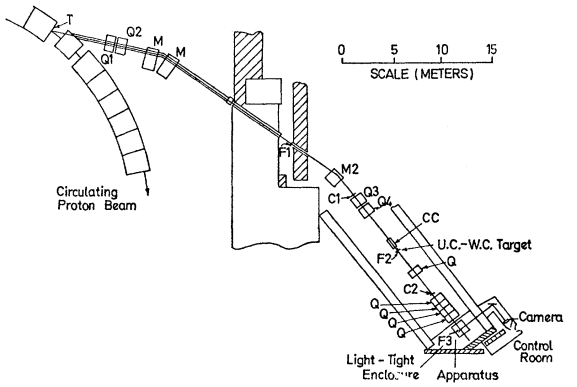

FIG. 1. Over-all layout of the experiment, together with the π-meson beam used.

with a relatively small amplitude from s-channel resonances: this was demonstrated by the results of a calculation using a particular model. Such models have since been extended by several other authors,[3–5] who have made widely varying assumptions about the s-channel resonances. We show in Sec. 5 how the results vary so much that this seems an unrewarding procedure. It would seem that conclusions about these resonances can only be deduced with adequate certainty from detailed phase-shift analyses of all the available data, including these angular distributions. However, the fact that a good fit can be made using the Regge model, with no free parameters, remains and is an interesting and surprising result. In the present paper we present details of our angular distributions.

In a previous paper[6] we presented some particular results from a study of the reaction

$$\pi^-+p\rightarrow\pi^0+\pi^0+n. \tag{3}$$

We showed that there are two important mechanisms contributing to this reaction at our energies:

(i) the isobar production reaction noted earlier [Eq. (2)];

(ii) peripheral production of the dipion system, which we took to be due to $\pi\pi$ scattering, deducing some interesting results about the s-wave $\pi\pi$ interactions.

In the present paper we present our final results. In addition to more details and elaboration of the results published earlier,[2,6] we present

(i) total cross sections for the different possible channels;

(ii) measurements of the reaction

$$\pi^-+p\rightarrow n+(\eta^0\rightarrow 2\gamma). \tag{4}$$

At higher momenta ($\gtrsim$2.9 GeV/c), this reaction has also been found to fit with a Regge model. However, in contrast to our measurements of reactions (1) and (2), the Regge model for reaction (4) with the parameters found to fit at higher momenta is not successful in fitting our data;

(iii) measurements of

$$\pi^-+p\rightarrow n+3\gamma, \tag{5}$$

which we take to be due to the reaction

$$\pi^-+p\rightarrow n+\pi^0+\gamma. \tag{6}$$

In other measurements of this latter reaction it was assumed that it is due to production of the ω^0 meson, followed by its neutral decay to produce $\pi^0+\gamma$. It would seem that only about 30% of our cross section for reaction (6) is due to this mechanism, with the remainder due to other processes; we suggest direct radiative processes, with some indication that some diffraction dissociation process is providing part of the cross section.

In the course of this work it was necessary to develop a broad range of new techniques. This was particularly so in the data analysis, where we had to develop procedures for subtraction of the background due to failure to detect all γ rays produced in an event, and procedures to obtain kinematic information from the directions of the γ rays. An account of these techniques is presented.

2. EXPERIMENTAL DETAILS

The over-all layout of the experiment is shown in Fig. 1.

A. Beam

A high-density target T of dimensions 6×1×1 cm was bombarded by the internal proton beam of Nimrod. Negative particles produced at an angle of 20° were brought to a focus at F1, where a collimator roughly defined the beam momentum and removed stray particles in the beam halo. The momentum bite was actually defined by the aperture of the quadrupole Q4, in conjunction with bending magnet M2. At the second focus F2, the beam passed through the 5-cm-diam liquid-hydrogen target used by the University College–Westfield College (London) collaboration,[7] who were studying π^-p elastic scattering. The beam was refocused at F3, 11 m downstream, onto our hydrogen target: a 3-cm-diam vertical cylinder of nylon with 0.025 cm wall thickness. The walls of the vacuum vessel were of 0.05-cm stainless steel, with beam entry and exit windows of 0.025-cm Mylar.

[3] A. Yokosawa, Phys. Rev. **159**, 1431 (1967).
[4] J. Baacke and M. Yvert, Nuovo Cimento **51A**, 761 (1967).
[5] S. Minami, Nuovo Cimento **52A**, 577 (1967).
[6] I. F. Corbett, C. J. S. Damerell, N. Middlemas, D. Newton, A. B. Clegg, W. S. C. Williams, and A. S. Carroll, Phys. Rev. **156**, 1451 (1967).
[7] E. H. Bellamy, T. F. Buckley, W. Busza, D. G. Davis, B. G. Duff, F. F. Heymann, P. V. March, C. C. Nimmon, A. Stefanini, J. A. Strong, R. N. F. Walker, and D. T. Walton, Proc. Roy. Soc. (London) **A289**, 509 (1966).

In the absence of aberrations in the beam magnets, and with no material in the beam, the spot size expected at F3 was 1×1 cm. The measured spot size was 1.8×3.3 cm, due largely to multiple scattering in beam-defining counters for the two experiments, although aberration effects (particularly in Nimrod's fringe field) are also a significant factor. The relative intensities at F1, F2, and F3 were 1.00, 0.54, and 0.43, respectively.

The intensity at F3 was $600\pi/10^{11}$ protons incident on T. During data-taking the intensity of the internal beam was roughly $2\text{–}3\times10^{11}$ protons/pulse with a pulse repetition frequency of 26/min. The beam spill time was typically 200–300 msec, although there was considerable structure, reducing the effective spill time to about 30 msec. The lepton contamination of the beam at F3 is estimated to be 0.062 ± 0.020, based on a measured contamination of 0.033 ± 0.014 at CC, where a gas-filled Čerenkov threshold detector could be raised into the beam for this purpose, and an estimate of the increase due to pion decay between CC and F3.

B. Counters

A diagram of the detection system is shown in Fig. 2. The incident beam was defined by counters C1, C2, and C3, made of 0.3-cm-thick NE102 plastic scintillator with shapes tailored to the beam profile. The Perspex light guides of counters C1 and C2 were oriented to minimize coincidences caused by Čerenkov light produced by particles in the beam halo; for the same reason C3 had an air light-guide. An interaction producing a neutral final state was identified by a veto counter C4, covering a solid angle of 3.84π sr around F3: It consisted of a cylinder of 0.6-cm-thick NE102 plastic scintillator which was 20 cm high and 14.6 cm in diameter with a hemispherical bottom dome, and had a 2×3 cm beam-entry window. C4 performed throughout the experiment with high efficiency, only about 0.1% of our trigger rate being attributable to its inefficiency.

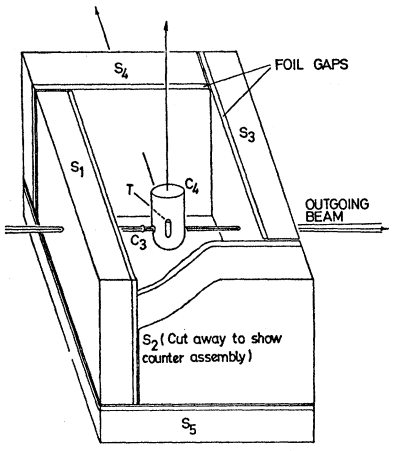

FIG. 2. Diagram of the arrangement of the hydrogen target (T), the final two counters (C3–4), and the five detecting spark chambers (S1–5).

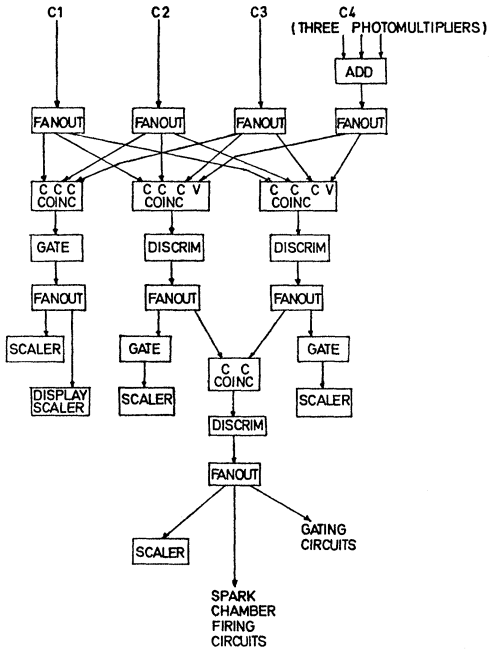

FIG. 3. Block schematic of electronics.

C. Spark Chambers

To study the γ rays produced in these neutral interactions the target was surrounded on five sides by spark chambers, each containing ten brass plates of thickness 3.41 g cm^{-2}. In addition, each chamber had two thin aluminum foil plates on the face towards the hydrogen target, to ensure rejection by the scanners of any charged particle entering the chambers. The chambers subtended 3.32π sr at F3, and presented a minimum of 1.8 conversion lengths[8] of material to a γ ray.

Two orthogonal views of each chamber were photographed by a pulse-operated Flight Research camera. Choice of camera aperture was difficult, because of the need to record faint sparks while not losing spatial resolution, due to film halation, for bright sparks. This intensity problem was aggravated by the need to use a chromatic filter to reduce the considerable chromatic aberration caused by the large distance between field lens and spark chambers. These conflicts were adequately resolved using Kodak R60 film at an aperture of f8, with an orange Barr and Stroud filter type OY2; the demagnification factor of the optical system was 52×.

D. Electronics

Our trigger logic requirement was simply $C_1C_2C_3\bar{C}_4$. However, since the cross section $\sigma(\bar{\pi}^- p \rightarrow \text{neutrals})$ is only ~3 mb in this momentum range and our target contains ~0.2 g cm^2 of hydrogen, only 1 in 2000 pions satisfies this criterion. Therefore it was neces-

[8] A conversion length is defined as the thickness in which a proportion $(1-e^{-1})$ of the γ rays convert.

TABLE I. Scanning hierarchy.

Class	Description
I	Spurious triggers, not originating in fast logic.
II	Rejected frames: beam renormalization required. SubClassifications: (a) Fiducial failure (b) Camera advance failure (c) Multiple incoming beam tracks (d) A spark chamber not triggered.
III	Background triggers: subclassifications (a) Beam halo (b) Pion interacts in the entry spark chamber (c) Interactions producing charged particles in counter C_3 (d) γ-ray conversions before spark chambers (e) Strange-particle production (f) Veto failures
IV	Event Classified according to number of γ rays observed.

sary to investigate events that simulate the trigger requirement.

The block schematic of electronics finally chosen is shown in Fig. 3. (Unless stated otherwise, all units are standard AERE or RHEL units.) It was found that, in a single channel, time-slewing effects became apparent when pulse separations of ~10 nsec occurred (for approximately 1 in 3000 pions). However, these effects were not the same for different units, and it was found that, if the logic requirement $C_1C_2C_3\bar{C}_4$ was formed twice with two different systems and their outputs put in coincidence to form the final trigger, the number of false triggers due to such causes was reduced to an unimportant level. The only complication of this scheme arises from the relative normalization of all channels. This was measured by taking periodic counts of $C_1C_2C_3$ on all channels: a beam-normalization correction of 1.148 ± 0.031 was indicated.

The over-all delay between an event and spark formation in the chambers was ~450 nsec. The chambers were run with a clearing field of 20 V, giving a memory time of ~1 μsec. The recovery time-constant of the high-voltage supplies to the spark chambers was 23 msec, and the camera cycle time was (nominally) 60 msec. The dead time of 79 msec used was therefore adequate for recovery of the system. It was found, however, that the pulsed fiducial lights, which were being run rather hard because of the low transparancy of the orange filter for the xenon discharge, became somewhat unreliable when operated several times per beam burst. A small percentage of our pictures had to be rejected owing to these failures.

E. Data Collection

Data were collected at pion momenta of 1.72, 1.89, 2.07, 2.27, and 2.46 GeV/c. Approximately equal time was spent at each momentum, and approximately 40% of our time was used for empty-target runs. A typical data-taking cycle started with a short run taking 300 photographs with trigger $C_1C_2C_3$ to study the profile of the beam tracks, followed by four long runs with trigger $C_1C_2C_3\bar{C}_4$, the target being full and empty on alternate runs. The cycle was terminated with another beam-profile run. Beam momenta were changed approximately every 24 h.

3. DATA REDUCTION

Each frame of film was scanned, classified, and measured at one viewing. A small sample (~2%) of film was rescanned later to determine the scanning efficiency, and to locate biases in the measured data.

The measured data were then passed through a two-stage computer analysis system. The first stage did the data checking and geometrical reconstruction; for each event the directions of the observed γ rays, in three dimensions, were then recorded as our primary event library on magnetic tape. The second stage produced an expanded library of events and "mock events" such as would be produced if any combination of γ rays had not been observed. We will show in outline below how this secondary event library is used to eliminate the effects of partial geometrical coverage and incomplete conversion of γ rays from the results. This final library tape could then be passed through any filtering and histogramming routine of the SUMX type in order to study any class of event.

A. Scanning and Measuring

The film was projected, with a magnification of 38×, onto the measuring table. This had a central turntable rotatable through 360°, on which was mounted a sliding cursor plate. Both movements were mechanically coupled to rotary digitizers whose coordinates could be transferred to paper tape by operating a foot switch.

The scanner classified each frame according to the hierarchy shown in Table I and made an entry on the scan sheet. The total number of pictures which fell into each category are shown in Table II.[9] For a Class IV classification the scanner made the same entry, using a typewriter keyboard, onto paper tape as an event signature code, and then carried out the following measurements: (i) two fiducial lines; (ii) the two orthogonal views of the beam track; (iii) the positions of the first spark of each shower in each view, ensuring that when there was more than one shower in a chamber the ordering of measurements in each chamber was the same. The measuring sequence was designed to economize on effort and time required by the scanner.

It is worth stressing here the usefulness of such a measuring machine in spark-chamber physics. The availability of either line or point measurement with the same hardware allows a flexible measuring program

[9] Owing to a misprint, the total number of pictures used was previously recorded (Ref. 6) incorrectly as 1 700 000.

to be devised, keeping measuring time down. Typically 100 frames/h were processed, with approximately one-half of these requiring measurement.

Daily measurements of the projector calibration were made, using a standard film grid. These also served as a check of mechanical and electrical reliability from projector to paper-tape punch. Periodically, all fiducial lines were measured to ensure that no unexpected changes in mirror positions, etc., had taken place.

At the end of each run, a summary of the scanning sheets was made. Since class I tended, for hierarchical reasons, to be overpopulated in the scanning results, the true number of class-I events was deduced from the difference between the number of triggers supplied by the fast logic, and the number of pictures actually taken. The two main ambiguities with class I are classes IId and IIIa. If there was any class-I excess it was reallocated to these classifications in proportions dictated by comparison with nearby runs in the time sequence which did not have this excess of class-I frames. A possible beam normalization error of $\sim 2\%$ may arise from this procedure.

B. Geometrical Reconstruction

Data from the measuring tables were passed through the first-stage analysis in batches of several runs. First, the measurements for each event were checked for format: any failure was noted on the line-printer output, which also produced a listing of all accepted events for bookkeeping purposes. The trajectory of the beam particle was then deduced and if the result did not pass through C_3, the event was rejected. Finally, the coordinates of the shower vertices were calculated in turn, and if any vertex was shown not to be in the chamber stipulated by the event code, or if the two views gave discrepant coordinates, the event was rejected, the reason again being noted. The best estimate of the interaction point is the point $(x',y',0)$, where the beam vector intersects the mid-plane of the hydrogen target. The origin of the coordinate system was then transferred to $(x',y',0)$ and the resulting coordinates of the direction vector of the beam track and of the shower vertices were recorded in our event-magnetic-tape library.

The basic reconstruction grid used consisted of a set of four location parameters, two scaling and two distortion parameters for each view of each chamber: a total of 80 parameters, which allowed a reconstruction accuracy of ± 2 mm. This was adequate for the shower vertices, but was not sufficiently accurate for the beam geometry. For these a further eight parameters were included, enabling the beam trajectory to be reconstructed with a positional accuracy of ± 0.3 mm, and an angular accuracy of ± 3 mrad.

Some initial analysis besides the bookkeeping was also done on the data at this stage, primarily for reasons of quality control. Most of this has no significance here, since its only function has been to signal malfunction of measuring equipment. Two things, however, are of over-all significance: the beam profile that is compiled for each run and the conversion depth distribution, which was used to obtain an early estimate of the effective plate thickness, which was then used in the second stage of analysis. The first point will be discussed more fully when considering beam-normalization problems below. The estimated thickness of one brass plate obtained (0.185 ± 0.006 conversion lengths) was in good agreement with our design figure of 0.20 conversion length. It was also found that the last gap of the spark chambers was inefficient, reducing the number of effective plates from nine to 8.4. These figures were used in the weighting calculation of the second stage of analysis.

TABLE II. Bookkeeping: classification of pictures taken.

Class	Experimental conditions: Target full	Target empty	All data
I	1300	300	1600
II	30 900	11 700	42 600
III	28 600	17 200	45 800
IV	51 600	15 400	67 000
Totals	111 100	44 300	155 400

Similar procedures were adopted for processing the beam profile data. Besides the beam profiles, which were needed for normalizing checks, these runs gave a valuable check on reconstruction accuracy. No entry was made on our event library tape for these pictures.

C. Production of Final-Data File

If a picture is observed with N γ-rays it may be due to an event with N γ rays or to an event in which $(N+M)$ γ rays were produced, of which M have either passed through the spark chambers without converting or have missed them. To study events in which N γ rays are produced, we have to deduce results from those pictures with N γ rays and then subtract a background deduced from those pictures with more than N γ rays. To do this we record, for each picture with n γ rays, the basic event with all γ rays together with a set of 2^n-2 mock events with all possible combinations of γ rays missed. With each of these events, real and mock are recorded a weighting factor such that, when we wish to study events of a given class it is only necessary to sum all such events on our library tape, either real or mock. This method is, in principle, exact in the limit of infinite statistics, and, for a finite sample, provides some sort of statistical best estimate of the true results. All the results we present have had the background due to incomplete detection subtracted in this way.

To obtain the weighting factors we first need to know the conversion efficiency. The values given above for the number of effective plates and their thickness gave a conversion efficiency for normally incident γ rays of

0.79 ± 0.01. Considered in more detail the conversion efficiency was a function of γ-ray energy, production angle, and azimuth, but, to keep analysis as simple as possible, we used a conversion efficiency averaged over the γ-ray energy spectra and the complete range of azimuth observable which provided adequate accuracy. This mean conversion efficiency was then fitted to a simple function of production angle. The deviations from this parametrization were less than 1%, except in regions of overlap between chambers where there might be departures up to 10%. These were, however, confined to a very small angular range and occurred in the regions where, because of large angles of incidence of the γ rays, the vertex tends to be fuzzy and ill-determined. It was not felt that any significant bias would arise from this simplification.

We now outline the details and justification of this analysis. For any observed event the appropriate weight is

$$W_m{}^m=[G_m(\theta_i,\phi_i)\prod P_i(\theta_i)]^{-1}, \tag{7}$$

where m is the multiplicity of the event.

$G_m(\theta_i,\phi_i)$ is the geometrical detection efficiency, calculated as that fraction of 2π over which an azimuthal rotation of the event leaves all γ rays within the geometrical coverage of the apparatus and $P_i(\theta_i)$ is the conversion probability of the γ ray labelled with index i.

The weighting factor of a mock event with m' γ rays, deduced from a picture with m γ rays, is

$$W_m{}^{m'}=\frac{(-1)^{m-m'}}{G_{m'}(\prod_i P_i)}\Big[\prod_j(1-P_j)+\sum_k\frac{G_{m'+1}{}^k}{G_{m'+1}}\prod_{j\neq k}(1-P_j)$$
$$+\sum_{k,l}\Big(\prod_{j\neq k,l}(1-P_j)\Big)\Big(\frac{G_{m'+1}{}^kG_m{}^l}{G_{m'+1}}+\frac{G_{m'+1}{}^lG_m{}^k}{G_{m'+1}}-G_m{}^{kl}\Big)$$
$$+\cdots\Big]. \tag{8}$$

The index i runs over all m γ rays in the parent picture, the index j runs over these γ rays which are left out in the mock event, and k runs over those γ rays in the parent picture which can be lost in the hole as the event is rotated azimuthally. G_a denotes that fraction of azimuthal angle for which all the γ rays in the set lie within the geometrical coverage, while $G_{m'+1}{}^{k,\text{ etc.}}$ denotes that fraction for which the set m' lies within the geometrical coverage and, γ rays k, etc., outside.

We illustrate this procedure by considering the fate of N interactions each producing four γ-rays with the same configuration, two of which (labelled with 1, 2) have production angles within the range of incomplete geometrical coverage. In our raw data we would observe the following numbers of events of different configurations (for N large and assuming the azimuthal distribution of the events to be random):

$$N(4,1234)=P_1P_2P_3P_4(\phi_0/2\pi)N,$$
$$N(3,123)=P_1P_2P_3(1-P_4)(\phi_0/2\pi)N,$$
$$N(3,124)=P_1P_2(1-P_3)P_4(\phi_0/2\pi)N,$$
$$N(3,134)=\{P_1(1-P_2)P_3P_4(\phi_0/2\pi)+P_1P_3P_4(\phi_2/2\pi)\}N,$$
$$N(3,234)=\{(1-P_1)P_2P_3P_4(\phi_0/2\pi)+P_2P_3P_4(\phi_1/2\pi)\}N,$$
$$N(2,12)=P_1P_2(1-P_3)(1-P_4)(\phi_0/2\pi)N,$$
$$N(2,13)=P_1P_3(1-P_2)(1-P_4)(\phi_0/2\pi)N+P_1P_3(1-P_4)(\phi_2/2\pi)N,$$
$$N(2,14)=P_1P_4(1-P_2)(1-P_3)(\phi_0/2\pi)N+P_1P_4(1-P_3)(\phi_2/2\pi)N,$$
$$N(2,34)=P_3P_4(1-P_1)(1-P_2)(\phi_0/2\pi)N+P_3P_4(1-P_2)(\phi_1/2\pi)N+P_3P_4(1-P_1)(\phi_2/2\pi)N+P_3P_4(\phi_{12}/2\pi)N,\ \text{etc.} \tag{9}$$

where ϕ_0, ϕ_1, ϕ_2, ϕ_{12} are the azimuthal ranges over which neither γ ray, γ ray No. 1, γ ray No. 2, and both γ rays, respectively, fall within the hole in the detector as one rotates the event about the beam. The notation otherwise is self-explanatory.

The weight applied to the four-γ events on transfer to the final-data library is just $(P_1P_2P_3P_4\phi_0/2\pi)^{-1}$, so we obtain the correct number of events in this category. For the procedure to work, when we sum all other events listed, the results must be zero. Consider the case for $N(2,14)$. The weight assigned to these events is $(P_1P_4\phi/2\pi)^{-1}$, where ϕ is simply the azimuthal aperture of the hole (which was essentially independent of the production angle for the range where it is not zero). Then on our final data file we have the following number of events:

$$N'(2,14)=N(2,14)W_2{}^2(2,14)+N(3,124)W_3{}^2(124,14)+N(3,134)W_3{}^2(134,14)+N(4,1234)W_4{}^2(1234,14),$$

and from 8, 9 we have

$$N(2,14)W_2{}^2(2,14)=\Big(P_1P_4(1-P_2)(1-P_3)\frac{\phi_0}{2\pi}+P_1P_4(1-P_3)\frac{\phi_2}{2\pi}\Big)\frac{2\pi N}{P_1P_4\Phi},$$
$$N(3,124)W_3{}^2(124,14)=-(1-P_3)(\phi_0/\Phi)\times((1-P_2)+\phi_2/\Phi)N,$$
$$N(3,134)W_3{}^2(134,14)=-[(1-P_2)\phi_0+\phi_2][(1-P_3)N/\Phi],$$
$$N(4,1234)W_4{}^2(1234,14)=\frac{\phi_0}{\Phi}\Big((1-P_2)(1-P_3)+(1-P_3)\frac{\phi_2}{\phi_0}\Big)N, \tag{10}$$

so that $N'(2,14)\equiv0$.

It is a straightforward matter to show that this method is generally true (though it would fail for certain configurations; for example, with four γ rays distributed uniformly in azimuth in the region of the hole the geometrical efficiency would be zero; however, events with such tightly defined configurations should be rare.) We have also compromised for the relatively small number of events with more than three γ rays in the range of production angle containing the hole. The calculation of the relevant geometrical factors becomes time-consuming at that stage, so we simplified by assuming azimuthal independence. Also, one further approximation was made. There were occasional high-multiplicity events with extremely low detection probability (maybe only 0.01), which can produce wild statistical fluctuations in any data using largely high-multiplicity events. We have therefore generally ignored the very few events with weights greater than 100.

Our final analyses of different classes of events use selection routines through which all events on our final-data file are passed, histogramming the relevant distribution functions. The details of these programs will be discussed in Sec. 5, where we present our experimental results. During summation, it was assumed that each picture had unit statistical weight. Therefore, the error assigned to a bin containing n events, real and mock, with weights W_i is just $\pm(\sum_{1=i}^{n} W_i^2)^{1/2}$. This procedure ignores the correlation between the errors for the mock events deduced from the same picture. In general, the binning on our histogram is fine enough that the probability of two or more mock events contributing to the same bin is negligible. This approximation is better when we make some selection, for example, when we select charge-exchange events by placing a cut on the opening angle distribution. This procedure is, however, clearly incorrect when we calculate total cross sections for producing each multiplicity of γ rays. Therefore, in that case, we assign the correct contribution $(\sum W_i)^2$ to the squared error for all the mock events deduced from a single picture. Any more detailed handling of the errors on histograms would demand a prohibitive amount of computation. That our approximation is adequate is confirmed by the way our histograms have fluctuations about smooth curves which are consistent with the assigned errors.

4. EXPERIMENTAL BIASES, ERRORS, AND UNCERTAINTIES

Before describing our experimental results we survey here the possible biases introduced at various stages in our analysis. The over-all statistics of our data processing have already been summarized in Table II. About 27% of our pictures were rejected for various reasons as unsuitable for measurement. This involves a considerable renormalization of our raw electronic event rates, so we have paid careful attention to biases that might arise. A more detailed breakdown of our data, by momenta, is given in Table III. Errors can arise both at the scanning stage and as a result of the rejection of measured data by our stage-1 analysis programs. We consider the two problems separately. Finally, we discuss other possible errors and biases and summarize our over-all normalization uncertainty.

TABLE III. General statistical information.

Target condition	P_{π^-} (GeV/c)	No. of pictures taken (thousands)	No. of events measured (thousands)	No. of events accepted (thousands)
H_2	1.71	32.3	12.6	12.1
	1.89	22.6	10.0	9.6
	2.07	21.6	10.4	9.9
	2.27	17.6	8.7	8.3
	2.46	17.1	10.0	9.7
Empty	1.71	14.5	4.1	3.9
	1.89	8.2	2.8	2.7
	2.07	8.2	3.1	2.9
	2.27	7.0	2.5	2.4
	2.46	6.5	2.8	2.7

A. Scanning Biases

2200 frames were rescanned to obtain information on scanning efficiencies and biases. Details of the intercomparison are shown in Table IV. Although approximately 12 months separated the two scans there was agreement in detailed classification for 90% of the data. In 139 cases different hierarchical classes were assigned, largely owing to changes in the largely subjective judgement as to frame measurability (class II) changing the effective total beam for the two scans. Taking this into account, the event rates for the two scans agree within $(0.5\pm1.2)\%$. We have allowed a normalization factor of 1.00 ± 0.02 to take this uncertainty into account.

More serious from the point of view of subdivision of cross section into different channels was the fact that for the 1089 agreed events, the γ-ray multiplicities were in agreement in only 1015 cases. On inspection it was found that in $(3.1\pm1.1)\%$ of events there was a recognizable neutron interaction. The scanning efficiency for these interactions, however, was only 0.38 ± 0.23, so that in $\sim1.2\%$ of our events a neutron interaction has been classified as a γ ray. Better statistical information on this point was obtained by inspecting our events with three measured vertices, for those cases which were consistent with the hypothesis of a charge-exchange interaction in which a neutron interaction was measured and interpreted as a γ ray. This showed that $(1.60\pm.6)\%$

TABLE IV. Scanning efficiency checks.

Class	Scan 1	Scan 2	Agreement
II	609	567	539
III	498	507	459
IV	1119	1152	1089

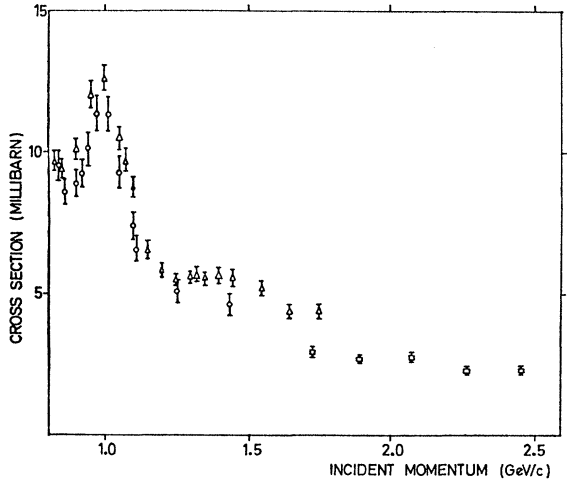

FIG. 4. Total cross sections for production of neutral final states. The measurements shown are from □, this experiment; △, Ref. 10; ○, Ref. 11.

of our charge-exchange interactions came within this classification. It is assumed that this figure applies to events of all γ-ray multiplicities.

In the remaining 5.7% with discrepant classifications, it appeared that the simplest explanation was a finite scanning efficiency for γ-ray-induced showers. If this was 0.995 ± 0.005 good agreement with the observed results (90% χ^2 probability) was obtained for the multiplicity distribution of events with discrepant classification. This scanning efficiency, and the equivalent effect of the "measuring efficiency" discussed below, have to be folded with the measured conversion efficiency to obtain the detection efficiency used in compiling our final-data file.

B. Measuring Biases

In processing the data from the measuring table, a small fraction (1.8%) of events were not accepted by the computer because of tape-punching errors. These events will clearly have a bias as the probability of this is proportional to the number of measurements made. A further 1.8% were rejected because the reconstructed beam track did not pass through the hydrogen target. A comparison between the rates of these latter events with the target filled with liquid hydrogen, and empty, showed that a genuine background effect is involved. Finally 0.8% of our events failed due to inconsistencies in vertex measurements: again the bias is against events with a large number of γ rays in a given spark chamber. In total 2.6% of our events were not accepted for further analysis, for reasons that can introduce biases in the γ-ray multiplicity distribution. The effect is taken into account by assigning a "measuring efficiency" of 0.99 to each γ ray.

TABLE V. Correction and renormalization factors.

1. Beam normalization uncertainty due to scanning and measuring losses	$1.00\ \pm0.020$
2. Electronic rates correction	1.048 ± 0.031
3. Lepton contamination	1.062 ± 0.020
4. Hydrogen vapor correction	1.017 ± 0.000
5. Target thickness uncertainty	1.000 ± 0.011
6. δ-ray production	1.010 ± 0.000
7. Multiplicity-dependent factors,	
(a) $\pi^0\rightarrow e^+e^-\gamma$;	$1.012\pm0.001/\pi^0$
(b) γ-ray conversion in hydrogen target.	$1.045\pm0.005/\gamma$
Mean correction factor: (mean No. of π^0/event $=1.6\pm0.2$; mean No. of γ rays $=3.5\pm0.3$)	
Over-all correction factor	1.338 ± 0.063

TABLE VI. Total cross section for $\pi^-p\rightarrow$ neutrals.

Momentum (GeV/c)	Cross section[a] (mb)
1.71	2.95 ± 0.07
1.89	2.74 ± 0.07
2.07	2.77 ± 0.07
2.27	2.30 ± 0.06
2.46	2.30 ± 0.05

[a] Note that, in addition to the statistical uncertainty shown, there is an additional uncertainty of 5%, made up of a 4% uncertainty in the normalization and 3% from uncertainty in the estimate of the mean γ-ray multiplicity of our events.

C. Conversion Efficiency

All showers converting in chambers 1 and 3 (see Fig. 2) were used in a more extended study of the conversion efficiency of our apparatus. A maximum-likelihood method was used, treating separately events of a given multiplicity in each of the two chambers (both of which can affect the mean γ-ray energy). No significant difference was found between the conversion efficiencies deduced for each of these groups, in agreement with estimates that the conversion efficiency should not vary with γ-ray energy down to a minimum energy, below which γ rays were not detected. The mean plate thickness found was 0.191 ± 0.003 conversion units. This was slightly larger than the figure used in stage-II analysis. After correction for scanning and measuring efficiencies, however, we arrive at the figure used. Furthermore, by recalculating a sample of our data with a modified conversion efficiency, we found that the changes introduced were an order of magnitude smaller than the statistical uncertainties.

TABLE VII. Number of pictures with no γ rays, both observed and deduced from pictures with one or more γ rays (expressed as pictures/10^6 pions incident).

Momentum (GeV/c)	Observed	Deduced
1.71	18.0 ± 1.8	17.8 ± 1.8
1.89	8.4 ± 1.6	12.1 ± 1.6
2.07	10.5 ± 1.45	9.9 ± 1.4
2.27	5.3 ± 1.22	6.4 ± 1.2
2.46	4.3 ± 0.9	6.1 ± 0.9
Sum	46.4 ± 3.2	52.3 ± 3.2

TABLE VIII. Cross sections (in μb) observed for producing different numbers N of γ rays.

N \ Incident momenta (GeV/c)	1.71	1.89	2.07	2.27	2.46	Average
1	214± 78	139± 73	125± 65	28± 56	58± 45	113± 29
2	1373±137	1002±134	869±121	735±110	674± 91	931± 53
3	372±177	499±174	602±164	488±161	496±136	493± 73
4	647±205	831±203	883±191	544±200	587±171	698± 87
5	344±231	141±213	243±201	484±209	126±198	267± 94
6	322±297	162±225	−22±199	46±219	398±219	201±101
7	−299±326	98±113	317±193	8±222	−74±193	10± 99
8	271±230	18± 67	−236±206	−10±164	136±132	36± 76
9	−72± 72	−3± 27	188±153	57± 57	−34± 69	27± 39
10			−51± 51		21± 21	−6± 11

D. Effective Target Thickness

This was measured by the beam-profile runs. Within the statistical accuracy all runs gave the same value for the mean target thickness, 2.50±0.02 cm. Because of the small target size, local bubble formation due to heat losses was a possibility. During construction of the target it was confirmed visually that this did not occur. We have taken the hydrogen density to be 0.0708 ±0.0007 g/cm^2. To correct for the presence of hydrogen vapor in the empty target vessel we alter our normalization by 1.017±0.000.

E. Loss of Low-Energy γ Rays

As we accept two sparks or more as a γ-ray shower, we estimate that our conversion efficiency will be constant with energy down to a minimum energy of about 20 MeV. (Important contributions to the conversion efficiency come from the Compton effect at lower energies.) This estimate of constant conversion efficiency is supported by the results described in Sec. 4 C.

Therefore, some events will be recorded as having a lower multiplicity than the true value due to failure to observe one or more low-energy γ rays. We have made estimates of the order of magnitude of this effect and found that it is small. No corrections have been made for this in the results presented.

F. Other Effects

There are a number of other effects which have to be considered. Some of these are independent of event multiplicity (such as the production of δ rays by the incident pion which can veto the event). Others depend on the number of neutral pions, such as Dalitz pair production, or on the γ-ray multiplicity, such as conversion before reaching the spark chambers. Numerical values for these and all other correction factors previously measured are listed in Table V.

5. EXPERIMENTAL RESULTS

A. Total Neutral Cross Sections

Our values for this cross section are given in Table VI. These results are derived from our scanning records. As we include as an event at this stage the pictures with no visible γ ray, our detection efficiency is 100%. The only point at which our subsequent analysis enters is through the estimate of the mean multiplicity for events which determine the normalization factor in Table V. Figure 4 shows how our results compare with other measurements.[10,11] The results from the two spark-chamber experiments (ours and that of Chiu *et al.*[11]) are lower than those from the pure counter experiment of Brisson *et al.*,[10] possibly owing to a greater ability to sort out backgrounds from the spark-chamber pictures.

B. Cross Sections for Different Multiplicities

The cross sections presented here are the results of our weighting procedure, described in Sec. 3 C. First, however, we compare in Table VII the number of pictures in which no γ rays are observed with those we deduce should be observed from our analysis of pictures with one or more γ rays. The good agreement between these provides some support for our weighting procedure: The difference between the two columns corresponds only to a cross section of about 13 μb.

In Table VIII we show the cross sections for producing different numbers of γ rays, from one to ten, deduced by the weighting procedure from the observed multiplicities. The sums of these cross sections are in good agreement with the results in Table VI, which were obtained independently of our weighting procedure. We also quote the average cross section (over our five momenta) for each multiplicity, as this displays the over-all pattern of the results. We see that the cross section for producing events with more than three neutral pions is small, in agreement with the small production of more than three charged pions at these energies. Some of the $3\pi^0$ production will be due to production of the η^0 meson. We will see, in Sec. 5 D,

[10] J. C. Brisson, P. Falk-Vairant, J. P. Merlo, P. Sonderegger, R. Turlay, and G. Valladas, in *Proceedings of the Aix-en-Provence International Conference on Elementary Particles, 1961*, edited by E. Cremlen-Alcan *et al.* (Centre d'Etudes Nucleaires de Saclay, Seine et Oise, 1961), p. 45.

[11] C. B. Chiu, R. D. Eandi, A. C. Helmholz, R. W. Kenney, B. J. Moyer, J. A. Poirier, W. B. Richards, R. J. Cence, V. Z. Peterson, N. K. Sehgal, and V. J. Stenger, Phys. Rev. **156**, 1415 (1967).

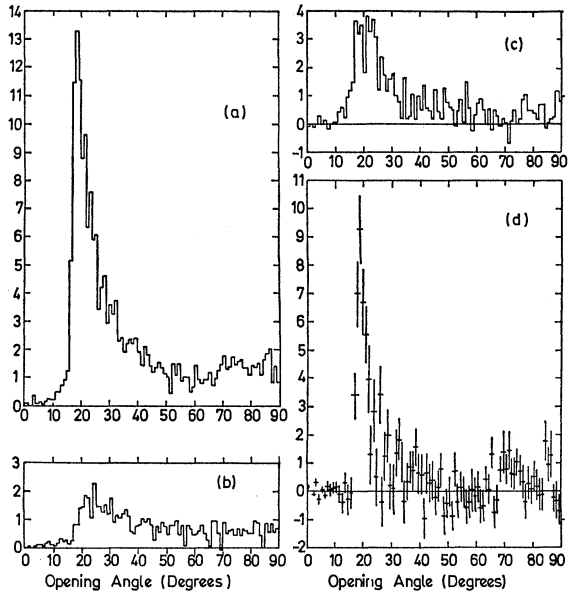

FIG. 5. Distributions of opening angles (in degrees) observed for two γ-ray events at 2.07 GeV/c. (a) Observed distribution for all two γ-ray pictures from full target. (b) The distribution for two γ-ray pictures, from full target, due to incomplete detection of higher multiplicity events; deduced as described in Sec. 4 C. (c) Distribution for two γ-ray events from empty target. Here the background due to incomplete detection of higher-multiplicity events has been subtracted. (d) The result of subtracting (b) and (c) from (a): our estimate of the true distribution which would be observed from a target of pure hydrogen with a detecting system of complete efficiency. The ordinate throughout is (weighted events)/(10^6 incident π mesons). So as not to clutter the figures we have only plotted the statistical errors in (d).

that the average cross section for production of this meson followed by its decay into two γ rays is 118 ± 16 μb. From the known branching ratios,[12] we deduce a cross section of 86 ± 12 μb for production of the $3\pi^0$ decay mode of the η^0 meson, which implies that an important part of the $3\pi^0$ production is due to production of the η^0 meson.

We see that, as well as production of even numbers of γ rays, which can be due to production of π^0 mesons, there is evidence for production of 3γ and 5γ states. The former can be due to production of the ω^0 meson followed by its neutral decay: $\omega^0\rightarrow\pi^0\gamma$. We shall see, in Sec. 5 G, that our cross section is too large to be due solely to this process, and that there is evidence that other processes are involved. However, one can ask whether our observed production of odd numbers of γ rays is really due to production of even numbers, followed by failure to observe some γ rays due to some inefficiency or to adding a false γ ray, due to some noise. We have considered such possibilities, as described in Sec. 4, and found no evidence for them. We will see, in a later section, how our results agree with another measurement of production of 3γ events, as well as with other measurements of 2γ events. A result which argues for such a trouble is the indication, in Table VIII, of an unreasonably large cross section for production of single γ rays. This cross section should be twice the cross section for the reverse reaction

$$\gamma+n\rightarrow p+\pi^-,$$

which one would expect to be similar to the cross section for the process

$$\gamma+p\rightarrow n+\pi^+.$$

Interpolating between measured cross sections, one would estimate a cross section of the order of 10 μb for this latter process, suggesting a cross section of the order of 20 μb for production of single γ rays. This result suggests that there is, in this channel, a background of events with incorrectly identified multiplicity corresponding to a cross section of approximately 90 μb. In the zero γ-ray class the corresponding background is only of the order of 10 μb, while from the fits to the opening angle distributions for 2γ events (described below) we deduce that the background there is less than 100 μb (90% confidence level). We therefore think it unlikely that in any other channel the background of events with incorrect multiplicity is more than 100 μb.

C. Opening Angle Distributions

If we are observing the reaction

$$\pi^-+p\rightarrow x^0+n,$$

the particle labelled as x will have a unique velocity v in the c.m. system of the reaction. If x then decays isotropically into two γ rays, as will a π^0 meson or an η^0 meson, the distribution of opening angles α between the pairs of γ rays is given by

$$P(\alpha)=\frac{\cos\frac{1}{2}\alpha}{2\beta\gamma\sin^2\frac{1}{2}\alpha(\gamma^2\sin^2\frac{1}{2}\alpha-1)^{1/2}},$$

where $\beta=v/c$ and $\gamma=(1-\beta^2)^{-1/2}$. This distribution has

TABLE IX. Tables of J_n, smearing coefficients for angular distributions for an incident momentum of 2.07 GeV/c.

n	$\pi^-p\rightarrow\pi^0n$	$\pi^-p\rightarrow\eta^0n$
0	1.000	1.00
1	0.997	0.96
2	0.992	0.90
3	0.984	0.80
4	0.973	0.70
5	0.960	0.60
6	0.945	0.47
7	0.927	0.38
8	0.908	...
9	0.886	...
10	0.863	...
11	0.837	...
12	0.812	...

[12] I. Butterworth, in *Proceedings of the Heidelberg International Conference on Elementary Particles, 1967* (North-Holland Publishing Co., Amsterdam, 1968), p. 11.

a sharp peak at the minimum opening angle allowed:

$$\sin\tfrac{1}{2}\alpha_{\min}=\gamma^{-1}.$$

To improve our statistical accuracy we combine the opening angle distributions found at all five momenta, distorting the angular scales so that peaks due to mesons of the same mass will fall on top of each other. In detail, if

$$\xi=1/\sin\tfrac{1}{2}\alpha,$$

where α is the opening angle, we plot events as a function of

$$\mu=E_0\xi-(E_0^2\xi^2-E_0^2+M^2)^{1/2},$$

where E_0 is the total energy available and M is the mass of the neutron. Then μ is a mass such that if a particle of this mass decays into two γ rays the distribution of opening angles will peak at the corresponding value of α. Thus by observing such peaks in the opening angle distribution one can identify events from production of different mesons.

In passing we remark that this peak in the opening angle distribution for a monoenergetic π^0 meson means that the opening angle between the pair of γ rays from the decay of a π^0 meson provides a rather good estimate of the energy of the meson, for a large proportion of decays. We use this fact in our analyses of events with three and four γ rays.

Knowing solely the directions of the two γ rays, we cannot determine the true direction of the parent meson; the best estimate available to us is the bisector of the γ-ray directions. This bisector will be distributed with azimuthal symmetry about the true direction and at an angle θ to it. Writing

$$\lambda=\cos\theta,$$

the probability of the estimated direction being between λ and $\lambda+d\lambda$ is

$$f(\lambda)=\frac{\lambda d\lambda}{\gamma^2(1-\beta^2\lambda^2)^{3/2}(1-\lambda^2)^{1/2}},$$

where β, γ are as above. This will produce a smearing of the angular distribution, which, as this probability is independent of azimuth about the true direction, is similar to the smearing of an angular distribution due to studying it with cylindrical counters, such as has been studied in low-energy experiments. It has been shown[13] that if the true angular distribution is expanded in Legendre polynomials,

$$G(\theta)=\sum_n a_n P_n(\cos\theta),$$

and the smearing function is independent of azimuth about the true direction, as $f(\lambda)$ above, the experimental angular distribution is

$$G_{\text{expt}}(\theta)=\sum_n a_n J_n P_n(\cos\theta),$$

where

$$J_n=\int_0^{\lambda_{\max}} f(\lambda)P_n(\lambda)d\lambda.$$

TABLE X. Cross sections for productions of mesons decaying into two γ rays.

Incident momentum (GeV/c)	π^0 meson (μb)	η^0 meson (μb)	"950-MeV meson" (μb)
1.71	1158±63	153±39	42±29
1.89	840±55	85±37	47±32
2.07	673±47	155±37	50±31
2.27	565±41	110±31	45±28
2.46	538±34	86±28	69±23

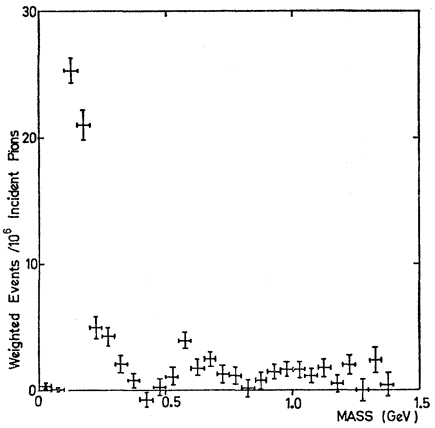

FIG. 6. Average opening angle distributions for two γ-ray events. In adding the opening angle distributions at our five momenta the horizontal scale has been adjusted so that peaks from decay of a meson will fall on top of each other, as described in the text. The horizontal scale is such that the minimum opening angle from decay of a meson is labelled with the mass of the meson.

To deduce angular distributions we have selected events only in the peaks of the opening angle distributions, making cuts which would accept 70% of π^0 mesons and 80% of η^0 mesons. (These cuts were chosen to optimize the statistical accuracy; increasing the upper limit increased the background which had to be subtracted). For such cuts, at an incident momentum of 2.07 GeV/c, we calculate the values of J_n in Table IX, where we see that the smearing of the π^0-meson angular distributions is small, but that it is important for the η^0-meson angular distributions.

We show our opening angle distributions, for an incident momentum of 2.07 GeV/c, in Fig. 5. Figure 5(a) shows the opening angle distribution found for all real two γ rays events with target full, while Fig. 5(b) shows the corresponding background distribution, for full target, due to mock events, deduced as described in Sec. 3 C. Figure 5(c) shows the opening angle distribution for empty target, with the background due to mock events subtracted. The final distribution, with both backgrounds subtracted, is shown in Fig. 5(d); the

[13] M. E. Rose, Phys. Rev. 91, 610 (1953).

normalization is the same in all four of these figures. In Fig. 5(d) we see the pronounced peak due to the π^0 meson and indication of the η^0 meson.

The result of summing our five opening angle distributions is seen in Fig. 6, where we see peaks due to the π^0 meson and to the η^0 meson and an indication that there are events which could correspond to decay of a meson of mass about 950 MeV.

D. Cross Sections for Two γ-Ray Events

To deduce best estimates of the total cross sections for producing different mesons we made least-squares fits to the opening angle distributions, assuming them to be made up of contributions due to the π^0 meson, the η^0 meson, and to a meson of mass 950 MeV. Fits were made assuming uncertainties in the opening angle of 1° and 1.5°: these were found to be equally satisfactory, with no significant differences between the cross sections deduced (it will be obvious that the uncertainty in opening angles is smaller than the uncertainties in directions of the individual γ rays). The results, assuming an uncertainty of 1°, are presented in Table X,

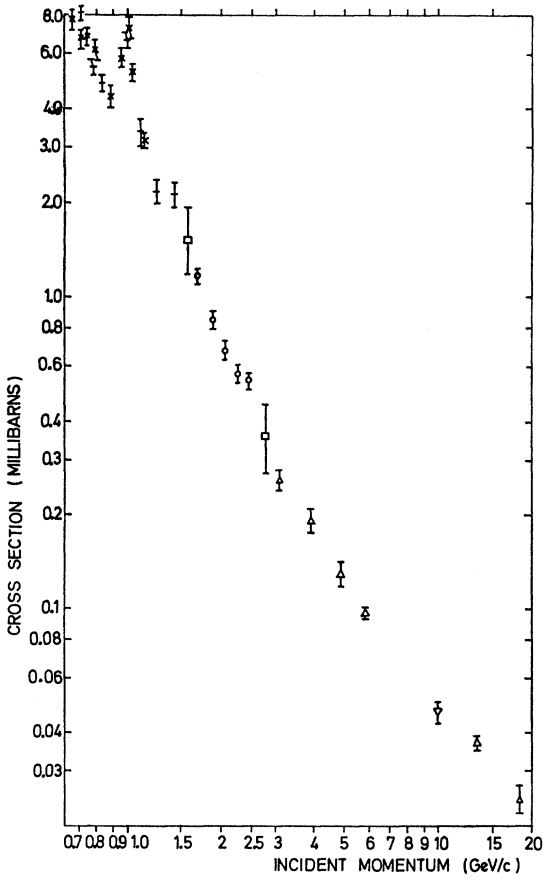

FIG. 7. Excitation function for the reaction $\pi^- p \to \pi^0 n$, for incident momenta from 0.65 to 18.2 GeV/c. The measurements displayed are from: ○, this experiment; +, Ref. 11; ×, Ref. 14; □, Ref. 15; △, Ref. 16; ▽, Ref. 17.

where the cross sections are for production of the meson followed by its decay into two γ rays.

In Fig. 7 we show the excitation function for charge-exchange scattering,

$$\pi^- + p \to \pi^0 + n.$$

In addition to our results, from Table X, we show results of Chiu *et al.*[11], Bulos *et al.*,[14] Barmin *et al.*,[15] Sonderegger *et al.*,[16] and Wahlig and Mannelli.[17] We see that the consistency of all these results is very good, and that there is no visible peaking in our energy region.

Our total cross sections for η^0-meson production are plotted in Fig. 8, together with results of Richards *et al.*,[18] Bulos *et al.*,[19] and Guisan *et al.*[20] We see that all the cross sections for momenta greater than 1.7 GeV/c lie on a straight line on this log-log plot. The straight line in Fig. 8 is the result of a least-squares fit to these higher momentum results, assuming

$$\sigma = A p^{-n}$$

yielding $n = 1.54$. Such a value of the exponent has been shown[21] to be typical of meson-exchange processes.

One can speculate that the suggestion of a meson of mass about 950 MeV decaying into two γ rays might be due to such a decay mode of the η' meson of mass 957 MeV, which is known to decay primarily into $\pi\pi\eta$. The average cross section for the reaction

$$\pi^+ + n \to p + [\eta' \to \pi^+ + \pi^- + (\eta^0 \to \text{neutrals})]$$

has been measured[22] in our energy range. Combining these results with the η' branching ratios of Rosenfeld

[14] F. Bulos, R. E. Lanou, A. E. Pifer, A. M. Shapiro, M. Widgoff, R. Panvini, A. E. Brenner, C. A. Bordner, M. E. Law, E. E. Ronat, K. Strauch, J. Szymanski, P. Bastein, B. B. Brabson, Y. Eisenberg, B. T. Feld, V. K. Fischer, I. A. Pless, L. Rosenson, R. K. Yamanoto, G. Calvelli, L. Guerriero, G. A. Salandin, A. Tomasini, L. Ventura, C. Voci, and F. Waldner, Phys. Rev. Letters **13**, 558 (1964).

[15] V. V. Barmin, A. G. Dolgolenko, Yu. S. Krestnikov, A. G. Meshkovskii, and V. A. Shebanov, Zh. Eksperim. i Teor. Fiz. **46**, 1426 (1964) [English transl.: Soviet Phys.—JETP **19**, 102 (1964)].

[16] P. Sonderegger, J. Kirz, O. Guisan, P. Falk-Vairant, C. Bruneton, P. Borgeaud, A. V. Stirling, C. Caverzasio, J. P. Guilland, M. Yvert, and B. Amblard, Phys. Letters **20**, 75 (1966).

[17] M. Wahlig and I. Mannelli, Phys. Rev. **168**, 1515 (1968).

[18] W. B. Richards, C. B. Chiu, R. D. Eandi, A. C. Helmholz, R. W. Kenney, B. J. Moyer, J. A. Poirier, R. J. Cence, V. Z. Peterson, N. K. Sehgal, and V. J. Stenger, Phys. Rev. Letters **16**, 1221 (1966).

[19] F. Bulos, R. E. Lanou, A. E. Pifer, A. M. Shapiro, M. Widgoff, R. Panvini, A. E. Brenner, C. A. Bordner, M. E. Law, E. E. Ronat, K. Strauch, J. J. Szymanski, P. Bastien, B. B. Brabson, Y. Eisenberg, B. T. Feld, V. K. Fischer, I. A. Pless, L. Rosenson, R. K. Yamamoto, G. Calvelli, L. Guerriero, G. A. Salandin, A. Tomasini, L. Ventura, C. Voci, and F. Waldner, Phys. Rev. Letters **13**, 486 (1964).

[20] O. Guisan, J. Kirz, P. Sonderegger, A. V. Stirling, P. Borgeaud, C. Bruneton, P. Falk-Vairant, B. Amblard, C. Caversazio, J. P. Guilland, and M. Yvert, Phys. Letters **18**, 200 (1965).

[21] D. R. O. Morrison, Phys. Letters **22**, 528 (1966).

[22] M. A. Abolins, O. I. Dahl, J. S. Danberg, D. Davies, P. Hoch, J. Kirz, D. H. Miller and R. Rader, paper presented at the Heidelberg Conference on Elementary Particle Physics, 1967 (unpublished); and J. Kirz (private communication).

TABLE XI. Charge-exchange differential cross sections.

$\cos\theta$ \ P_π	1.71 GeV/c (μb sr^{-1})	1.89 GeV/c (μb sr^{-1})	2.07 GeV/c (μb sr^{-1})	2.27 GeV/c (μb sr^{-1})	2.46 GeV/c (μb sr^{-1})
1.00	548±110	598±120	528±106	288±58	173±35
1.00– 0.95	435±54	415±60	452±57	337±50	313±42
0.95– 0.90	334±50	299±53	479±52	279±47	239±39
0.90– 0.85	322±48	174±49	203±42	119±42	114±31
0.85– 0.80	204±38	165±47	155±38	108±38	85±25
0.80– 0.75	160±40	66±36	78±32	76±27	53±26
0.75– 0.70	142±32	2±38	67±29	43±22	20±19
0.70– 0.65	42±30	30±30	19±23	59±21	57±17
0.65– 0.60	54±22	26±23	40±22	41±17	41±14
0.60– 0.55	33±22	−5±23	14±19	52±21	41±15
0.55– 0.50	37±23	42±18	26±19	43±19	57±18
0.50– 0.45	43±18	27±19	44±21	44±17	30±17
0.45– 0.40	66±23	52±19	46±22	70±19	49±16
0.40– 0.35	32±26	62±21	62±20	−1±19	46±16
0.35– 0.30	32±26	97±23	66±20	43±25	46±17
0.30– 0.25	101±33	138±31	46±25	76±20	52±15
0.25– 0.20	78±31	81±28	109±29	80±23	63±17
0.20– 0.15	101±37	91±26	27±27	53±21	65±17
0.15– 0.10	112±33	76±26	80±26	63±23	44±18
0.10– 0.05	141±36	67±40	19±26	47±21	43±16
0.05– 0	82±32	77±31	31±27	14±19	21±15
0 –−0.05	123±34	73±30	32±27	20±21	18±17
−0.05–−0.10	52±30	91±31	25±26	15±29	−26±18
−0.10–−0.15	63±34	65±29	49±21	26±16	12±16
−0.15–−0.20	71±40	−13±31	36±17	21±12	18±14
−0.20–−0.25	152±35	2±30	4±25	18±15	20±13
−0.25–−0.30	68±33	32±34	−19±18	−8±16	−6±13
−0.30–−0.35	61±33	5±32	−1±23	−9±20	37±12
−0.35–−0.40	11±29	38±36	51±22	−2±15	5±12
−0.40–−0.45	154±36	68±35	−1±31	43±20	41±14
−0.45–−0.50	78±38	68±30	6±29	73±22	16±18
−0.50–−0.55	54±39	37±32	−54±27	19±25	46±16
−0.55–−0.60	38±38	22±27	31±27	29±17	18±19
−0.60–−0.65	75±44	89±31	−36±31	−29±26	18±17
−0.65–−0.70	32±38	32±40	48±23	−65±27	−7±14
−0.70–−0.75	55±32	43±37	22±27	42±20	4±17
−0.75–−0.80	29±30	−5±32	9±22	9±15	38±18
−0.80–−0.85	19±32	39±26	13±29	−6±15	26±17
−0.85–−0.90	27±32	18±25	17±16	1±21	39±20
−0.90–−0.95	27±37	−18±37	75±29	−6±27	28±16
−0.95–−1.0	44±38	28±32	85±30	33±22	46±25

et al.[23] (Assuming that their branching ratio of (11±8)% to neutrals other than from $\pi\pi\eta$ to be all due to a $\gamma\gamma$ decay: (this assumption could, of course, produce an overestimate of the cross section), and branching ratios for the decay of the η meson,[12] we deduce an expected cross section for the reaction

$$\pi^- + p \rightarrow p + (\eta' \rightarrow 2\gamma)$$

of 16±12 μb. Therefore, it would seem that the effect indicated in Fig. 6 cannot be due to such a decay of the η' meson.

E. Bisector Distributions for Charge-Exchange Scattering

Our experimental bisector distributions are given in Table XI. These differential cross sections have been corrected for the selection on the opening angle distribution and for interaction of neutrons in the veto counter. This latter correction was only appreciable for

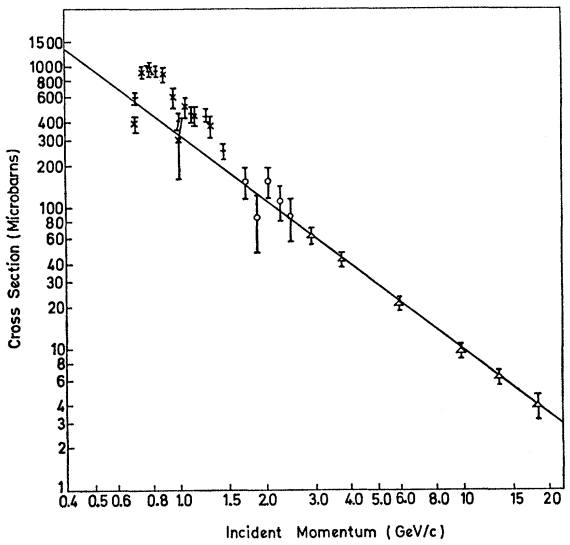

FIG. 8. Excitation function for the reaction $\pi^- p \rightarrow n(\eta^0 \rightarrow 2\gamma)$ from threshold to an incident momentum of 18.2 GeV/c. The measurements displayed are from ○, this experiment; + Ref. 18; ×, Ref. 19; △, Ref. 20.

[23] A. H. Rosenfeld, N. Barash-Schmidt, A. Barbero-Galtieri, W. J. Podolsky, L. R. Price, P. Soding, C. G. Wohl, M. Roos, and W. J. Willis, Rev. Mod. Phys. **40**, 77 (1968).

TABLE XII. Coefficients of Legendre polynomial expansion of bisector distribution for charge-exchange scattering (μb sr^{-1}).

Incident momenta / n \ (GeV/c)	1.71	1.89	2.07	2.27	2.46
0	81± 8	66± 7	49± 4	46± 6	40± 5
1	100±15	77±14	74± 8	75±11	66±11
2	88±21	41±20	90±11	70±15	75±14
3	100±24	98±22	64±13	61±17	60±16
4	99±27	86±24	123±15	68±20	58±17
5	29±29	109±28	79±16	58±21	62±19
6	−16±31	14±29	43±19	31±21	38±19
7	41±36	−19±31	1±20	−5±23	−29±20
8	4±36	0±34	19±21	4±24	−30±22
9	−20±41	30±35	−2±23	−9±26	−6±24
10	24±45	9±37	16±25	−57±29	−21±26
11	10±46	−16±37	21±24	−42±29	−74±26
12	24±49	50±40	−5±26	−22±31	−74±28

forward π-meson angles, where the neutrons have low energies, and was never greater than 10%. We remark that our measurements agree well with the measurements of Wahlig and Mannelli[17] where the two experiments overlap.

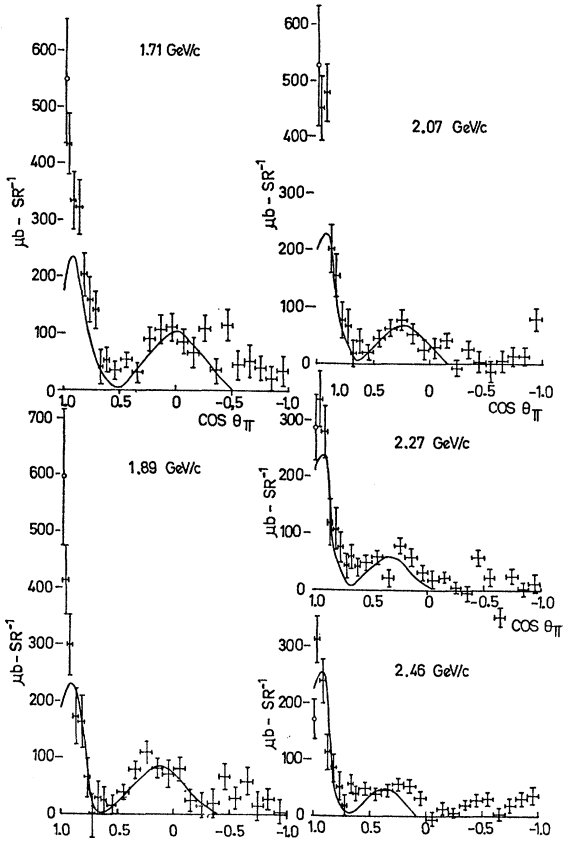

FIG. 9. Bisector angular distributions for charge-exchange scattering. Also plotted are the zero-degree cross sections from dispersion relations, adjusted as described in the text. The full curves show cross sections calculated by using the Regge-pole model to extrapolate from measurements at momenta from 5.9 to 18.2 GeV/c, assuming one form for the ρ-meson trajectory, as described in the text.

In making fits to the differential cross sections with an expansion in Legendre polynomials we also included the zero-degree cross section deduced from dispersion relations.[24] To use these cross sections, we had to adjust them because of the smearing introduced in converting to the bisector distributions. This was done by making a fit without any such adjustment, and then using the coefficients deduced to estimate the smearing, and hence the change in the zero-degree cross section. The zero degree cross sections, adjusted in this way, are included in Table XI. Errors have been attached to them to take into account our uncertainties in normalization and in adjustment for smearing. The results of Legendre polynomial expansions, $\sum_n a_n P_n(\cos\theta)$ with $n_{\max}=12$, are given in Table XII, where we used the adjusted zero-degree cross sections as well as our measurements. They show no particular variation in a small number of coefficients, such as would indicate that these coefficients are dominated by an important amplitude for a single resonance, as has been observed in $\pi^- p$ elastic scattering at these energies.[25,26] One speculates that there may be an interesting reason for this difference between elastic scattering and charge-exchange scattering.

Our differential cross sections are plotted in Fig. 9. They show a forward peak and a secondary peak as has been found[16,17] at higher momenta, from 5.9 to 18.2 GeV/c. These latter results have been fitted well (see typically Höhler *et al.*,[27] who give references to other work) assuming a Regge form for the cross section

$$d\sigma/dt = F(t)s^{2\alpha(t)-2}.$$

If we assume

$$\alpha(t)=0.55+0.96t$$

and the corresponding $F(t)$, which fits the high-energy results, we deduce differential cross sections at our energies, which are shown in Fig. 9. They agree well with the measurements, surprisingly so as the Regge model is expected only to be good at high energies. However, the agreement with the Regge model of the high-energy experiments is not perfect, as there is some uncertainty in extrapolating the secondary peak from the higher momenta to ours, owing particularly to uncertainties in $\alpha(t)$. For example if we assume

$$\alpha(t)=0.56+0.83t+0.14t^2,$$

which also fits at higher energies, and the corresponding $F(t)$, the calculated secondary peaks at our momenta are reduced by a factor of 2 from those shown in Fig. 9.

[24] G. Höhler, J. Baacke, J. Giesecke, and N. Zovko, Proc. Roy. Soc. (London) **A289**, 500 (1966).
[25] A. Yokosawa, S. Suwa, R. E. Hill, R. Esterling, and N. E. Booth, Phys. Rev. Letters **16**, 714 (1966).
[26] W. Busza, D. G. Davis, B. G. Duff, F. F. Heymann, C. C. Nimmon, D. T. Walton, E. H. Bellamy, T. F. Buckley, P. V. March, A. Stefanini, J. A. Strong, and R. N. F. Walker, Nuovo Cimento **52A**, 331 (1967).
[27] G. Höhler, J. Baacke, H. Schaile, and P. Sonderegger, Phys. Letters **20**, 79 (1966).

TABLE XIII. Coefficients of Legendre polynomial expansion of bisector distribution for $\pi^- p \to n(\eta^0 \to 2\gamma)$ (μb sr^{-1}).

Incident momenta / n	1.71	1.89	2.07	2.27	2.46
0	13.4± 3.6	8.8± 3.4	11.1±3.2	10.7±2.9	8.1±2.3
1	19.2± 6.7	12.1± 6.3	10.7±6.4	1.1±5.6	1.6±4.7
2	−4.6± 8.6	3.6± 8.0	15.9±7.7	2.8±7.1	11.5±6.0
3	−1.8±10.0	−2.3± 9.4	−0.9±8.6	−4.2±8.2	−4.5±6.9
4	−12.7±10.8	−11.6±10.3	−5.5±9.9	10.3±8.9	14.8±7.4

However, the forward peak is scarcely changed, so that its agreement with our measurements is more certain.

In addition to this uncertainty there are differences, from the calculated curve, which vary with momentum. Attempts[2–4] have been made to fit these variations by allowing s-channel resonances to interfere with the Regge pole amplitude, or[5] by allowing s-channel resonances to interfere with an amplitude for exchange of a real ρ meson. Assuming three resonances (at 1920, 2190, and 2360 MeV), we obtained a fit[2] only if the isobar at 2190 MeV had $J=l+\frac{1}{2}$. However, Phillips in a private communication and Baacke and Yvert[4] have shown that the strong difference we found between $J=l+\frac{1}{2}$ and $J=l-\frac{1}{2}$ is washed out if seven more, distant, resonances are added, with only their tails contributing at our momenta: The importance of such effects, which must be uncertain, therefore makes such calculations seem of doubtful value. There is dispute as to whether the real part of the no-spin-flip part of the Reggeized ρ-meson amplitude changes sign at $(-t)\simeq 0.2$ (GeV/c)^2. Yokosawa[3] concludes from an analysis of our data at 2.07 GeV/c that it does not; while Baacke and Yvert[4] conclude that it does, from an analysis of unpublished data at higher momenta. These conclusions follow from the differential cross sections at $-t\simeq 0.6$ (GeV/c)^2. We compare the calculated curves of Baacke and Yvert in Fig. 10 with our measurements, where we see agreement with no change in sign, effectively extending the conclusions of Yokosowa. (There is a discrepancy in Yokosawa's paper,[3] between the text and the caption to Fig. 2. We have assumed, as the simplest hypothesis, a simple misprint in the figure caption: the results then agree with those of Baacke and Yvert.) However, the higher-momentum data agree with a change in sign; we conclude that this discrepancy is most probably due to defects of the interference model. Such defects can be due to uncertainties in tails of distant resonances, uncertainties in the resonances to be assumed, and uncertainties in the Regge amplitude such as we have discussed. There is also the danger that there are probably double-counting problems as has been emphasized by Dolen, Horn, and Schmid.[28]

F. Bisector Distributions for η^0-Meson Production

These angular distributions are of much worse statistical accuracy. The results of Legendre polynomial fits, with $n_{\max}=4$, are given in Table XIII and the average of the five angular distributions is shown in Fig. 11. We have also calculated the angular distribution from the Regge fit found[29] at higher momenta (from 2.91 to 18.2 GeV/c). We assumed

$$\alpha(t)=0.34+0.35t,$$

though use of the other forms considered by Phillips and Rarita would make no important difference. The angular distribution, calculated at 2.07 GeV/c, was analyzed into Legendre polynomials and smeared with the coefficients in Table IX. These calculated angular distributions, unsmeared and smeared, are shown in Fig. 11 where we see that they definitely disagree with experiment which would seem to argue against the Regge amplitude being the dominant contribution at our energies. As the measured and calculated total cross sections are so similar, it would seem difficult to ascribe this difference solely to the adding of further amplitudes. One is therefore left with the puzzling indication that the Regge amplitude may still be the dominant amplitude in charge-exchange scattering at our low energies, but this seems not to be so for η^0-meson production. For this latter reaction the change from the dominance of the Regge amplitude seems to have taken place between 2.9 GeV/c and about 2.0 GeV/c.

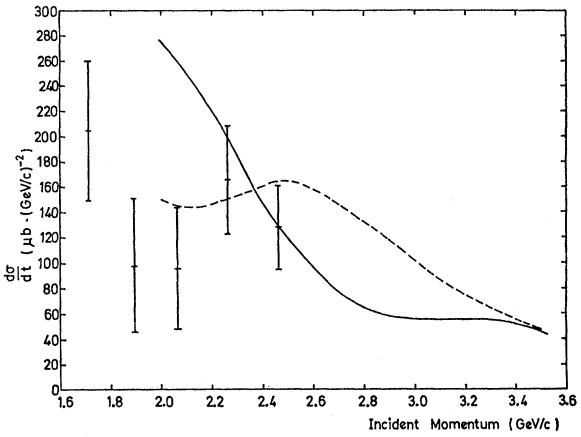

FIG. 10. Differential cross sections $d\sigma/dt$ for the reaction $\pi^- p \to \pi^0 n$ at $t=-0.6$ (GeV/c)^2, measured in this experiment. They are compared with calculations made by Baacke and Yvert (Ref. 4) using the interference model and assuming ——negative amplitude for no spin-flip – – –positive amplitude for no spin-flip.

[28] R. Dolen, D. Horn, and C. Schmid, Phys. Rev. Letters **19**, 402 (1967).

[29] R. J. N. Phillips and W. Rarita, Phys. Letters **19**, 598 (1965).

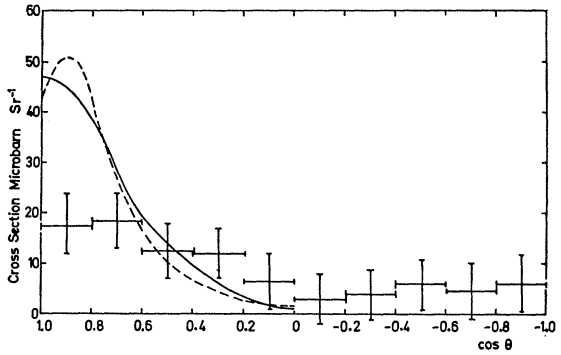

FIG. 11. Bisector angular distributions for the reaction $\pi^- p \to n(\eta^0 \to 2\gamma)$. The experimental points are the average over our five incident momenta, while the full line is calculated using the Regge-pole amplitude found (Ref. 29) to fit the higher energy data (Ref. 20) from 2.9 to 18.2 GeV/c. The calculated angular distribution before smearing is shown as the dashed curve.

G. Three-γ-Ray Production

We show in Fig. 12 the cross sections for production of three γ rays from Table VIII. Also shown are three cross sections, of a similar magnitude, from an experiment in a xenon bubble chamber.[30] Similar measurements of three-γ-ray production have been published,[31,32] though without quoting magnitudes of cross sections. Barmin *et al.*,[30,31] who work at energies close to ours, assume, implicitly, that the major contribution to production of three γ rays comes from

$$\pi^- + p \to n + (\omega^0 \to \pi^0 + \gamma).$$

We will show that only about 30% of our cross section comes from this process so that other processes, either real or misidentified as three gamma rays, are also involved. The results of Barmin *et al.*[30,31] at 2.8 GeV/c are similar to ours in both cross section and mass spectrum of the $\pi\gamma$ system so that a similar conclusion can be drawn there. [It is known[23] that $(9.7\pm1.8)\%$ of ω^0 mesons decay in a neutral mode and $\pi^0\gamma$ can be the only important contributor to this mode.] There will also be a contribution to three-γ-ray production from

$$\pi^- + p \to K^0 + [\Sigma^0 \to \gamma + (\Lambda^0 \to n + \pi^0)],$$

with the K^0 decaying in the K_L^0 mode outside our apparatus. The cross section for this is only 16 μb,[33] so its contribution will not be important. The possibility of direct radiative processes

$$\pi^- + p \to \pi^0 + n + \gamma$$

has been discussed recently,[34] and we will show that one such process is probably contributing.

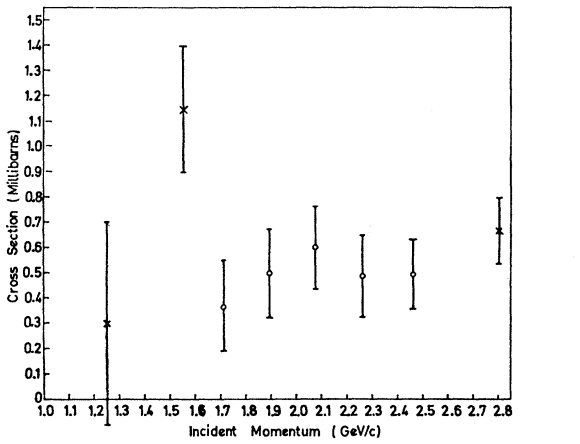

FIG. 12. Excitation function found for the reaction $\pi^- p \to n + 3\gamma$. Also shown are three measurements of Barmin *et al.* (Ref. 30).

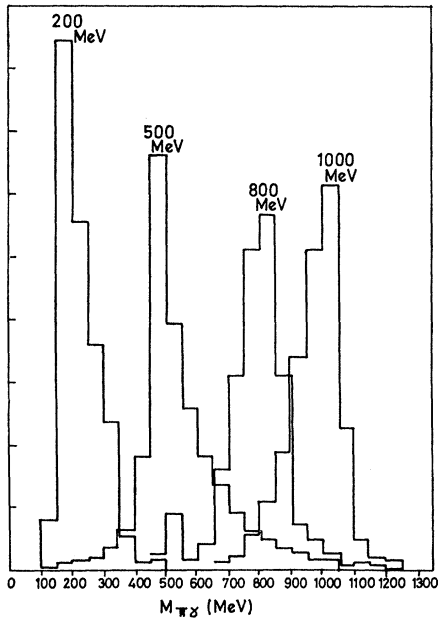

FIG. 13. $\pi\gamma$ mass distributions deduced, for the reaction $\pi^- p \to \pi^0\gamma n$, by our kinematical analyses procedure for events generated by the Monte Carlo procedure, assuming various unique masses for the $\pi\gamma$ system.

We assume that the three γ rays come from production of $\pi^0 + \gamma$, ignoring such possibilities as

$$\pi^- + p \to (\eta^0 \to 2\gamma) + n + \gamma.$$

The pair of γ rays with the smallest opening angle is assigned to the decay of the π^0 meson. We estimate the π^0 energy as

$$E = 154.0/\sin\tfrac{1}{2}\theta \text{ MeV},$$

where θ is the opening angle. This numerical constant

[30] V. V. Barmin, A. G. Dolgolenko, Yu. S. Krestnikov, A. G. Meshkovsky, Yu. P. Nikitin, and V. A. Shebanov, Phys. Letters **6**, 279 (1963); Zh. Eksperim i Teor. Fiz. **45**, 1879 (1963) [English transl.: Soviet Phys.—JETP **18**, 1289 (1964)].
[31] V. V. Barmin, A. G. Dolgolenko, A. G. Meshkovsky, and V. A. Shebanov, Phys. Letters **24B**, 249 (1967).
[32] E. Shibata and M. Wahlig, Phys. Letters **22**, 354 (1966).
[33] O. I. Dahl, L. M. Hardy, R. I. Hess, J. Kirz, D. H. Miller, and J. A. Schwartz, Phys. Rev. **163**, 1430 (1967).
[34] F. Chilton, D. Griffiths, and R. J. Jabbur, Phys. Rev. **153**, 1610 (1967).

was chosen so that for monoenergetic π^0 mesons the estimate will be within 10% of the correct energy for 90% of the decays. We estimate the direction of the π^0 meson as the bisector of the directions of the γ rays and then are able to deduce the remainder of the kinematic information for the reaction. In some cases the pair of γ rays are close together so that the energy deduced for the π^0 meson is larger than is kinematically allowed: We then take the second closest pair to be the π^0 meson, and in the rare cases for which even these are too close we switch to the third pairing. This repairing is most important when the mass of the $\pi\gamma$ system is small. This analysis procedure was tested by generating events by the Monte Carlo method. As an example the $\pi\gamma$ mass spectra deduced for various unique masses of the $\pi\gamma$ system are shown in Fig. 13. A similar resolution, of about 150 MeV, was also found for the πn mass.

In Figs. 14–16 we show the spectra obtained for the πn, γn, and $\pi\gamma$ masses; in each case these are the average of the data at our five momenta. The most

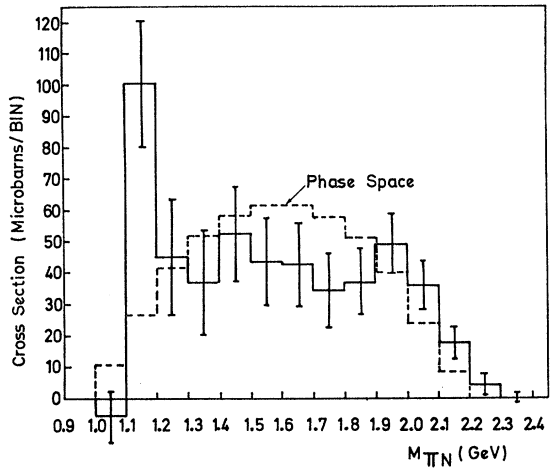

FIG. 14. πn mass spectrum observed for three-γ-ray events, taking them to be due to the reaction $\pi^- p \to \pi^0 \gamma n$. The results are the average over our five incident momenta; the phase-space curve is calculated for an incident momentum of 2.07 GeV/c and normalized to the same total cross section.

significant variation is in the $\pi\gamma$ mass spectrum which shows a broad hump about 400 MeV wide centered at about 700 MeV; we will see that this hump is made somewhat more significant on making a selection on γ-ray production angle to obtain Fig. 18(b). A similar broad hump is seen by Barmin *et al.*[31] at 2.8 GeV/c: this is also broader than their mass resolution.

We have compared our results with cross sections[22,35] for the reaction

$$\pi^+ + n \to \omega^0 + p.$$

The cross section for this reaction, with the ω^0 meson decaying in its neutral mode, is 140 μb (averaged across

[35] T. C. Bacon, W. J. Fickinger, D. G. Hill, H. W. K. Hopkins, D. K. Robinson, and E. O. Salant, Phys. Rev. **157**, 1263 (1967).

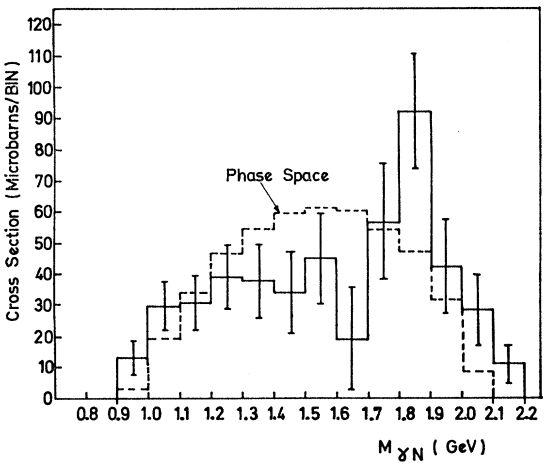

FIG. 15. γn mass spectrum observed for three-γ-ray events, taking them to be due to the reaction $\pi^- p \to \pi^0 \gamma n$. The results are the average over our five incident momenta; the phase-space curve is calculated for an incident momentum of 2.07 GeV/c, and normalized to the same total cross section.

our momenta) to be compared with the (493±73) μb we observe for production of three γ rays. We therefore conclude that only about 30% of our three-γ-ray production is due to ω^0-meson production.

We show evidence for a direct radiative process in Fig. 17. This is displayed differently in Fig. 18, where we show the $\pi\gamma$ mass spectra for forward γ rays in Fig. 18(a), and for other events in Fig. 18(b). To obtain an estimate of the $\pi\gamma$ mass spectrum corresponding to the forward γ-ray peak we have assumed the events in Fig. 18(b) to be an isotropic background and subtracted this estimate to obtain the results in Fig. 18(c). We see that the forward-peaked γ-ray angular distribution is associated with low $\pi\gamma$ masses. This result has the appearance of a diffraction dissociation process such as

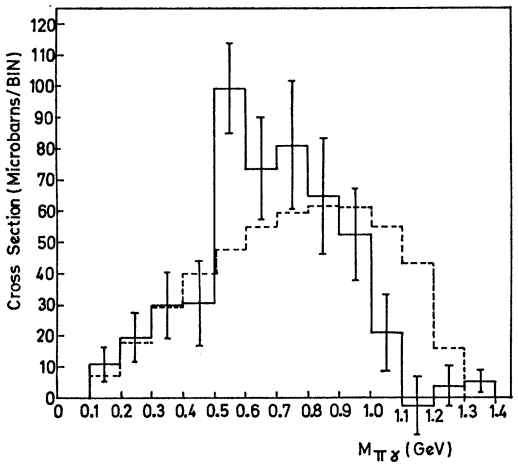

FIG. 16. $\pi\gamma$ mass spectrum observed for three-γ-ray events taking them to be due to the reaction $\pi^- p \to \pi^0 \gamma n$. The results are the average over our five incident momenta; the phase-space curve is calculated for an incident momentum of 2.07 GeV/c, and normalized to the same total cross section.

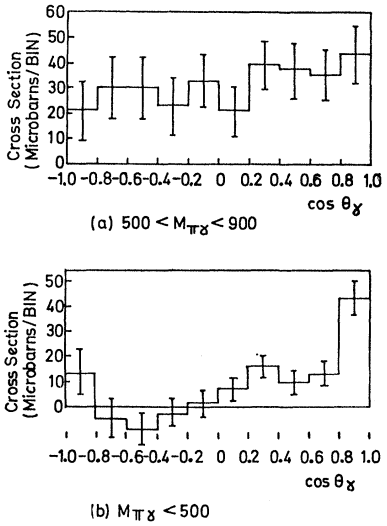

FIG. 17. γ-ray angular distributions found for the reaction $\pi^- p \to \pi^0 n\gamma$, for events selected for different ranges of mass of the $\pi\gamma$ system: (a) 500 MeV/c^2<$M_{\pi\gamma}$<900 MeV/c^2; (b) $M_{\pi\gamma}$<500 MeV/c^2. This shows how events with low mass of the $\pi\gamma$ system have a forward peaked angular distribution of the γ rays. The cross sections are averages over our five incident momenta.

has been suggested by Good and Walker,[36] in which a minimum transfer of momentum is made to the π meson, converting it to a $\pi\gamma$ system with low $\pi\gamma$ masses favored. The cross section we find for this process is of the order of 40 μb. Detailed models of this sort of process in other reactions have been discussed (see Ross and Yam[37] for recent work and references to earlier work); there still seems to be uncertainty as to what is happening in these processes, so that further study of this example should be rewarding. We show, in Fig. 19, the πn mass spectrum corresponding to this diffraction dissociation process. We see no structure in it: if the dominant mechanism were the pion-exchange process described by Chilton *et al.*,[34] we would expect to see the $N^*(1236)$. We have thus been able to explain about 200 μb of our production of three γ rays as due to ω^0-meson production, $\Sigma^0 K^0$ production, and this diffraction dissociation process, leaving about 300 μb to be explained. About 20 μb of this will be due to events in which two γ rays are detected together with a neutron misidentified as a γ ray, as we have shown earlier. We have been unable to find an explanation for the remainder: we can only think that there may be contributions from other radiative processes or from misidentified events of other multiplicities. It is to be emphasized that these events with three γ rays provide no clear-cut signature, such as we obtain for both 2γ and 4γ events. Similar remarks can be made about the indication of a number of 5γ events: They can also be due to other radiative processes or to events of other multiplicities, misidentified due to causes we have not discovered. We have attempted to study these 5γ events further, but, due to a combination of inefficiency of the procedures we have developed and the poor statistics, we have failed to obtain any useful information.

H. Four-γ-Ray Production

We have assumed that the main source of these events is the reaction

$$\pi^- + p \to \pi^0 + \pi^0 + n. \qquad (3)$$

We have developed an analysis procedure to obtain information about this reaction from the directions of the four γ rays. In most cases the pairs of γ rays from the two π^0 mesons are well separated and the bisector of each pair gives a good estimate of the π^0-meson direction. The opening angle between each pair gives a reasonable estimate of the energy of the π^0 meson and the two energies then provide a useful consistency check. This procedure has been described in detail elsewhere.[6,38] Because of cuts set to exclude events for which the above estimates were bad, about 75% of events from reaction (3) were accepted by this procedure; our cross sections have been corrected for this

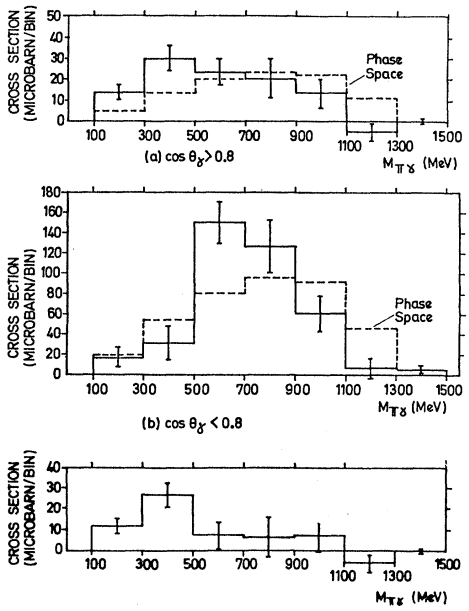

FIG. 18. $\pi\gamma$ mass spectra from the reaction $\pi^- p \to \pi^0 n\gamma$ for different ranges of γ-ray production angle: (a) $\cos\theta_\gamma > 0.8$; (b) $\cos\theta_\gamma < 0.8$; (c) shows the result of subtracting one-ninth of (b) from (a). In doing this we are estimating the $\pi\gamma$ mass spectrum corresponding to the forward peak in the γ-ray angular distribution by taking (b) to provide an estimate of an isotropic background, where θ_γ is the angle between the incident beam and the outgoing single γ ray, in the $\pi^- p$ c.m. system. All cross sections are averages over our five incident momenta; the phase-space curves in (a) and (b) are calculated for an incident momentum of 2.07 GeV/c and normalized to the same total cross-section.

[36] M. L. Good and W. D. Walker, Phys. Rev. **120**, 1857 (1960).
[37] M. Ross and Y. Y. Yam, Phys. Rev. Letters **19**, 546 (1967).
[38] A. S. Carroll, N. Middlemas, and W. S. C. Williams, Rutherford Laboratory Report No. RHEL/R104 (unpublished).

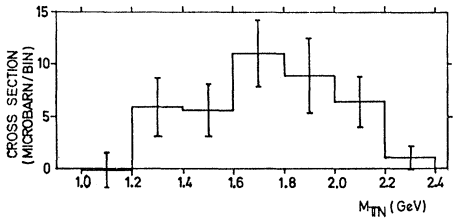

FIG. 19. πn mass spectrum from the diffraction dissociation process in the reaction $\pi^- p \to \pi^0 \gamma n$. This was deduced by selecting events with $M_{\pi\gamma} < 500$ MeV/c^2, and then, for these, subtracting one-ninth of the mass spectrum from events with $\cos\theta < 0.8$ from the mass spectrum from events with $\cos\theta > 0.8$, to obtain an estimate of the effect corresponding to the forward peak in the γ-ray angular distribution. The cross sections are averages over our five incident momenta.

inefficiency. A mass resolution of about 100 MeV for both $\pi\pi$ and πn systems was achieved. We also applied this analysis procedure to events generated by Monte Carlo methods from the reaction

$$\pi^- + p \to \pi^0 + (\eta^0 \to 2\gamma) + n \qquad (11)$$

and found that about 30% passed as if from reaction (3). They produced no peaking in any particular kinematic region of this reaction.

Our cross sections for producing four γ rays and for reaction (3) are given in Table XIV. There is an indication of a residue of events due to some other process than $\pi^0\pi^0$ production; they may be due to $\pi^0\eta^0$ production. We therefore developed an analysis procedure for $\pi^0\eta^0$ production, similar to that for $\pi^0\pi^0$ production and passed through it all events which failed the two-pion procedure (Note that as well as the residue in Table XIV, these will include a quarter of the $\pi^0\pi^0$ events.) We found no peaking in the $\pi^0\eta^0$, $\pi^0 n$, or $\eta^0 n$ mass spectra deduced. If the residue is due to $\pi^0\eta^0$ production about one-eighth of the events fitted as $\pi^0\pi^0 n^0$ will be due to this reaction; this background should be less important in the events selected as $N^*(1236)$ production or as peripheral dipion production.

We now summarize our previous results[2,6] and present some further results. $\pi^0\pi^0$ production shows relatively strong production of the $N^*(1236)$:

$$\pi^- + p \to \pi^0 + (N^{*0} \to n + \pi^0). \qquad (2)$$

We have shown[2] how the angular distribution for production of this isobar is very similar to that for charge-exchange scattering, suggesting that this N^* production is also due to exchange of a Reggeized ρ meson. In agreement with this conclusion it had previously been shown[39–42] how the alignment of the N^{*++} in the related reaction

$$\pi^+ + p \to \pi^0 + N^{*++}$$

corresponds to production by ρ-meson exchange. The extension of this to exchange of a Reggeized ρ meson has also been discussed by others.[43–45] We estimated the ratio of N^{*0} production to the spin-flip intensity in charge-exchange scattering by deducing the former by subtracting a background from the neighboring strip of the Dalitz plot as described in the next paragraph and in our previous letter[2] while the latter was deduced from the Regge-model fit to charge-exchange scattering shown in Fig. 9 decomposed into no-spin-flip and spin-flip parts as described in our previous letter.[2] The ratio obtained is 0.345 ± 0.082, which is in agreement with a ratio of 0.32 predicted from the quark model.[46]

We have investigated the decay angular distribution of the N^{*0} with respect to the exchanged system, which

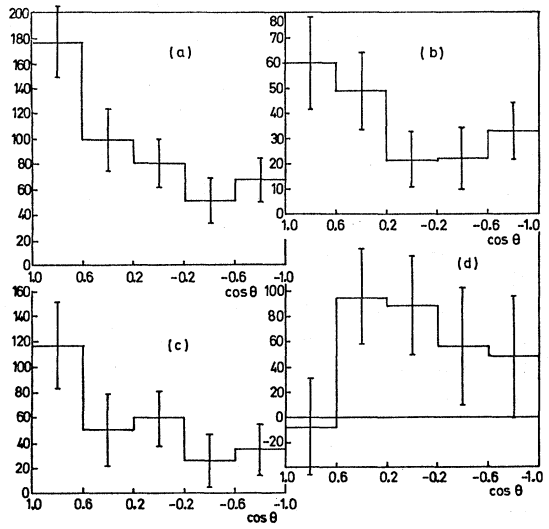

FIG. 20. N^{*0} decay angular distributions with respect to the incident π meson in the N^{*0} rest system, from the reaction $\pi^- p \to (N^{*0} \to n\pi^0)\pi^0$. In each case the $\pi^0 n$ system with the lower mass has been taken to be the N^*. (a), (b), and (c) are for $\cos\theta_\pi > 0.7$, where θ_π is the production angle of the recoil π-meson in the $\pi^- p$ c.m. system: (a) For all events with $1.2\ (\text{GeV}/c^2)^2 \leqslant M_{\pi n}^2 \leqslant 1.7\ (\text{GeV}/c^2)^2$; (b) the background intensity deduced from events with $1.7\ (\text{GeV}/c^2)^2 \leqslant M_{\pi n}^2 \leqslant 2.1\ (\text{GeV}/c^2)^2$, with normalization changed by the ratio of the areas of the strips on the Dalitz plot; (c) the result of subtracting (b) from (a); (d) The corresponding angular distribution, with background subtracted, for events with $\cos\theta_\pi < 0.7$.

TABLE XIV. Cross sections for four-gamma-ray events.

Incident momentum (GeV/c)	Total (μb)	$\pi^0\pi^0 n$ (μb)	Residue (μb)
1.71	647±205	616±93	31±229
1.89	831±203	609±94	222±227
2.07	883±191	701±88	182±214
2.27	544±200	305±85	239±218
2.46	587±171	486±69	101±188
Mean	698±87	544±39	153±95

[39] L. Stodolsky and J. J. Sakurai, Phys. Rev. Letters **11**, 90 (1963).
[40] N. Armenise *et al.*, Phys. Letters **13**, 341 (1964).
[41] M. Abolins *et al.*, Phys. Rev. **136B**, 195 (1964).
[42] M. Aderholz *et al.*, Nuovo Cimento **34**, 495 (1964).
[43] D. P. Roy, Nuovo Cimento **40**, 513 (1965).
[44] R. L. Thews, Phys. Rev. **155**, 1624 (1967).
[45] M. Krammer and U. Maor, Nuovo Cimento **50**, 963 (1967).
[46] J. L. Friar and J. S. Trefil, Nuovo Cimento **49A**, 542 (1967).

is expected[39–42] for ρ meson exchange to be of the form

$$1-0.5P_2(\cos\theta),$$

where θ is measured with respect to the incident pion, in the N^{*0} rest system. The angular distribution was deduced from the events with

$$1.2(\mathrm{GeV}/c^2)^2 \leqslant M_n^2 \leqslant 1.7(\mathrm{GeV}/c^2)^2$$

by subtracting a background intensity deduced from the events with

$$1.7(\mathrm{GeV}/c^2)^2 \leqslant M_n^2 \leqslant 2.1(\mathrm{GeV}/c^2)^2,$$

assuming that the density of the background was the same on these two strips of the Dalitz plot (in this calculation we always took the lower of the two possible πn masses). For events with $\cos\theta_\pi > 0.7$ (where θ_π is the production angle of the recoil pion in the $\pi^- p$ c.m. system), in the main peak of the production angular distribution (presented previously[2]) where ρ-meson exchange should particularly dominate, we show the raw angular distribution for events in the N^* band in Fig. 20(a), the background to be subtracted in Fig. 20(b), and the result of this subtraction in Fig. 20(c). A least-squares fit to this last distribution gives

$$(57.1\pm11.7)P_0(\cos\theta)+(45.6\pm21.0)P_1(\cos\theta) +(39.0\pm25.0)P_2(\cos\theta),$$

indicating both a P_1 term, inconsistent with decay of a pure resonance, and a P_2 term differing from expectation. That the angular distribution is really of the form $1-0.5P_2(\cos\theta)$ and the distribution in Fig. 20(c) is the result of a gross statistical fluctuation is not impossible, but it would seem that there is strong indication of further effects. In particular we think of interference with the background, neglected in subtracting it as an intensity, as has been discussed in other cases.[47,48] A possible such interference in this case has been discussed elsewhere,[49] based on the considerable kinematic overlap of this N^* production with peripheral production of dipions.

We also show, in Fig. 20(d), the decay angular distribution for N^* events with $\cos\theta_\pi < 0.7$, with background intensity subtracted. A least-squares fit gives

$$(55.5\pm18.8)P_0(\cos\theta)-(17.4\pm32.7)P_1(\cos\theta) -(27.0\pm34.5)P_2(\cos\theta),$$

which is consistent with ρ-meson exchange but is also consistent with many other possibilities.

We have previously[6] presented our measurements of peripheral dipion production and discussed their relation to s-wave $\pi\pi$ scattering. They show no indication of any narrow s-wave resonance, but, when interference with $I=2$ scattering is taken into account, are consistent with an $I=0$ phase passing slowly upwards through 90° in the $\pi\pi$ mass region of 700–800 MeV, consistent with recent analyses of the asymmetry in ρ^0-meson decay.[50,51]

ACKNOWLEDGMENTS

As the experiment described here was run on the proton synchrotron Nimrod of the Rutherford High Energy Laboratory, we are obviously very considerably indebted to very many people at that laboratory. We would particularly like to thank Dr. G. H. Stafford, D. C. Salter, and Dr. L. C. W. Hobbis and all his Nimrod Division. For data processing we used the facilities of the Atlas Computer Laboratory; we also wish to thank H. Hurst and J. Sparrow of the Rutherford High Energy Laboratory for their considerable help to us in this. We are also very happy to acknowledge our very considerable debt to Mrs. J. Huxtable and her scanners in Oxford.

[47] S. Goldhaber, J. L. Brown, I. Butterworth, G. Goldhaber, A. A. Hirata, J. A. Kadyk, and G. H. Trilling, Phys. Rev. Letters **15**, 737 (1965).

[48] R. W. Bland, M. G. Bowler, J. L. Brown, G. Goldhaber, S. Goldhaber, J. A. Kadyk and G. H. Trilling, Phys. Rev. Letters **17**, 939 (1966).

[49] A. B. Clegg, Nucl. Phys. **B6**, 75 (1968).

[50] E. Malamud and P. Schlein, Phys. Rev. Letters **19**, 1056 (1967).

[51] A. B. Clegg, Phys. Rev. **163**, 1664 (1967).